Appl. Math. Mech. -Engl. Ed., **43**(3), 311–326 (2022)

APPLIED MATHEMATICS AND MECHANICS (ENGLISH EDITION)

https://doi.org/10.1007/s10483-022-2829-9

A quasi-zero-stiffness isolator with a shear-thinning viscous damper*

Guilin WEN[1,2,†], Yu LIN[1], Junfeng HE[1]

1. School of Mechanical and Electrical Engineering, Guangzhou University, Guangzhou 510006, China;
2. School of Mechanical Engineering, Yanshan University, Qinhuangdao 066004, Hebei Province, China

(Received Aug. 19, 2021 / Revised Jan. 5, 2022)

Abstract Quasi-zero-stiffness (QZS) vibration isolators have been widely studied, because they show excellent high static and low dynamic stiffnesses and can effectively solve low-frequency and ultralow-frequency vibration. However, traditional QZS (T-QZS) vibration isolators usually adopt linear damping, owing to which achieving good isolation performance at both low and high frequencies is difficult. T-QZS isolators exhibit hardening stiffness characteristics, and their vibration isolation performance is even worse than that of linear vibration isolators under a large excitation amplitude. Therefore, this study proposes a QZS isolator with a shear-thinning viscous damper (SVD) to improve the vibration isolation performance of the T-QZS isolators. The force-velocity relation of the SVD is obtained, and a dynamic model is established for the isolator. The dynamic responses of the system are solved using the harmonic balance method (HBM) and the Runge-Kutta method. The vibration isolation performance of the system is evaluated using force transmissibility, and the isolator parameters are analyzed. The results show that compared with the T-QZS isolators, the proposed QZS-SVD isolator achieves the lower initial vibration isolation frequency and peak value, and exhibits better vibration isolation performance at medium and high frequencies. Moreover, the proposed isolator can withstand a large excitation amplitude in the effective vibration isolation range.

Key words quasi-zero-stiffness (QZS) isolator, shear-thinning viscous damper (SVD), vibration isolation, force transmissibility

Chinese Library Classification O322, O328
2010 Mathematics Subject Classification 74H45

1 Introduction

Vibration control has always been a key challenge in many engineering fields. The vibration isolation performance will considerably influence the performance of products, such as the res-

* Citation: WEN, G. L., LIN, Y., and HE, J. F. A quasi-zero-stiffness isolator with a shear-thinning viscous damper. *Applied Mathematics and Mechanics* (*English Edition*), **43**(3), 311–326 (2022) https://doi.org/10.1007/s10483-022-2829-9

† Corresponding author, E-mail: glwen@gzhu.edu.cn

Project supported by the Key Program of National Natural Science Foundation of China (No. 11832009), the National Natural Science Foundation of China (Nos. 11902085 and 12172095), and the Natural Science Foundation of Guangdong Province of China (No. 2021A1515010320)

olution of observation equipment for orbiting satellites, processing precision of machines, and riding comfort of running vehicles[1–5]. Vibration control is usually realized via active control, semi-active control, and passive control. Among these, passive control is the most considered and applied because of its simple structure and zero requirement for external energy. A traditional isolator is a linear system comprising mass, spring, and damper, and shows vibration isolation performance when the excitation frequency exceeds $\sqrt{2}$ times the natural frequency of the system. Generally, low-frequency vibration isolation performance can be enhanced by reducing the system stiffness. However, a system under low stiffness exhibits limited bearing capacity and stability[6]. Thus, it is difficult to achieve a balance between vibration isolation and bearing capacity.

To overcome the lack of low-frequency isolation performance in linear vibration isolators, quasi-zero-stiffness (QZS) isolators have been proposed as nonlinear systems[7]. Because of their high static and dynamic stiffnesses, QZS isolators can effectively compensate for the low-frequency passive vibration isolation. Carrrella et al.[8–9] established a classical three-spring QZS model, in which oblique and vertical springs were considered as the negative and positive stiffness elements, respectively. Kovacic et al.[10–11] studied the nonlinear dynamic behavior of this type of QZS isolator. Xu et al.[12] established models of four inclined and vertical springs, experimentally confirming the enhanced vibration isolation performance of the QZS isolator. In addition to inclined springs, many other types of structures have been designed to achieve the QZS. Lan et al.[13] used plane springs instead of inclined springs. Liu et al.[14] proposed a QZS isolator using an Euler buckled beam as the negative stiffness element. Niu et al.[15] reported a theoretical design and performed a characteristic analysis on the QZS isolator based on a disk spring as the negative stiffness element. Zhou et al.[16–18] designed a cam-roller mechanism to achieve the QZS characteristics of the vibration isolator. They designed a compact QZS rod, and extended the transmission of torsional isolations. Inspired by the shape of animal limbs, Zeng et al.[19] proposed a QZS isolator with a folded torsional spring structure. Moreover, magnetic springs have been studied by many researchers[20–23] and have been used to achieve the QZS.

Recently, research on QZS isolators has tended to be diverse. The performance of QZS vibration isolation systems has been further improved. Liu and Yu[24] added an auxiliary system to a three-spring QZS isolator to reduce its peak transmissivity and eliminate the jump phenomenon. Inspired by the bionic structure of the human body, Feng et al.[25] added a rotating unit with nonlinear inertia to an X-shaped structure to simulate the arm swing to reduce the resonance frequency of the system and achieve improved antiresonance characteristics. Yang et al.[26] proposed a QZS isolator with a nonlinear inertial mechanism, achieving improved low-frequency vibration isolation performance of the QZS isolator based on this mechanism. Lu et al.[27] analyzed a two-layer QZS vibration isolation system under harmonic excitation, experimentally verifying the improved performance of the high-frequency vibration isolation system. Wang et al.[28] established a two-layer QZS model with a cam-roller-spring mechanism. Zhao et al.[29] proposed that the nonlinear stiffness superposition of two pairs of inclined springs can be used to enhance the QZS region. Wang et al.[30] developed a double-layer QZS system with an ultrawide vibration isolation range. Deng et al.[31] fabricated a thirteen-level QZS isolator based on the stability characteristics of a bird's neck.

Alternatively, QZS isolators have been employed in various engineering practices. Kim et al.[32] designed a QZS isolator for an ultraprecision sensing system using a buckling plate as the negative stiffness element. Wang et al.[33] developed a type of baby carriage for neonatal transport using a pair of repulsive magnets in combination with linear springs as the positive stiffness element to obtain the QZS, which considerably reduced the vibration of infants during transport. Ding et al.[34] applied a three-spring QZS isolator to the vibration attenuation of a fluid-transmission pipeline.

The QZS isolators show better vibration isolation performance than linear systems owing

to their high static and low dynamic stiffnesses. However, some problems persist. If damping is increased to suppress the transmissibility near the resonance frequency, the high frequency transmissibility also increases, making it difficult to achieve good isolation performance at both low and high frequencies. Furthermore, the hardening stiffness of the QZS isolators will deteriorate the vibration isolation performance of the system under a large excitation amplitude. To solve these problems and further improve the vibration isolation performance of QZS systems, this study proposes a QZS isolator with a shear-thinning viscous damper (SVD). Previous studies have widely explored vibration isolation systems with a viscous damper. Lang et al.[35] and Lv and Yao[36] studied the influence of nonlinear viscous damping on a single-degree-of-freedom vibration isolation system, showing certain advantages of nonlinear vibration isolators over linear vibration isolators. Mofidian and Bardaweel[37] studied the influence of cubic nonlinear damping on the QZS system comprising magnetic inclined springs. They showed that nonlinear damping could eliminate frequency hopping, but the vibration isolation performance of this system was similar to that of a linear system at a low frequency. Liu et al.[38] proposed a QZS isolator with a viscoelastic damper, which further improved the high-frequency vibration isolation performance. However, the improvement in the low-frequency vibration isolation performance was not obvious. Zhang et al.[39] studied linear, nonlinear, and Bouc-Wen (BW) hysteretic dampings in a nonlinear vibration isolation system and explored the development of a broadband vibration isolation system. Unlike these studies, the present study applies an SVD to a QZS vibration isolator for the first time.

The remainder of this paper is organized as follows. In Section 2, the damping force characteristics of the SVD are analyzed, and a dynamic model is established for the QZS-SVD isolator. In Section 3, an analytical solution for the system is obtained using the harmonic balance method (HBM), and the solution is verified using numerical simulation. In Section 4, the superiority of the vibration isolation performance of the system is evaluated by comparing the force transmissibility of this system with that of the traditional QZS (T-QZS) vibration isolator, and the system parameters are analyzed. Finally, the conclusions of this study are summarized in Section 5.

2 Modeling of the QZS-SVD isolator

2.1 Damping force analysis of SVDs

Viscous fluids can be divided into Newtonian and non-Newtonian fluids based on whether the relation between the shear stress and the shear strain rate of the fluids conforms to Newton's inner friction law. Non-Newtonian fluids with rheological properties conforming to the power-law relation are called power-law fluids, which can be expressed as[40]

$$S = \eta D^n, \tag{1}$$

where η represents the viscosity coefficient, n denotes the flow index, and D denotes the shear velocity. η and n are constant. n determines the type of fluid. When $n = 1$, the fluid is deemed a Newtonian fluid, and η is the viscosity of the Newtonian fluid. When $n > 1$, the power-law fluid is called a shear-thickening fluid, and its viscosity increases with an increase in the shear rate. When $n < 1$, the power-law fluid is called a shear-thinning fluid, and its viscosity decreases with an increase in the shear rate. The damping of the QZS-SVD isolator is based on the shear-thinning fluid.

Based on the ideal mechanical model for a viscous damper with a shear-thinning fluid as the medium, the damping force is related only to the velocity and shows no stiffness storage effect. Based on the rheological characteristics of the fluid medium, the relation between the damping force and the velocity of the damper satisfies the power law[41], and thus, the force-velocity

relation can be expressed as

$$F_{\mathrm{d}} = cv^{\alpha}, \tag{2}$$

where F_{d} denotes the damping force produced by shear-thinning viscous damping, c represents the damping force coefficient, v denotes the response velocity, and α denotes the damping force index. Figure 1 shows the force-velocity curves under different values of α. When $\alpha < 1$, the force-velocity curve corresponds to shear-thinning viscous damping. In a small velocity range, an SVD can provide a larger damping force than a linear viscous damper, and a small value of α can yield a high damping force. In a large velocity range, the damping force of an SVD will be smaller than that of a linear viscous damper owing to the shear-thinning effect. The characteristics of shear-thinning damping determine the critical change point of damping ($v = 1$).

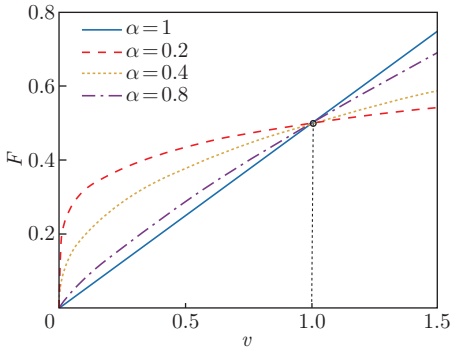

Fig. 1 Damping force-velocity curves under different values of α with $c = 0.5$ (color online)

When a vibration isolation system is subject to harmonic excitation, the periodic response of the system is

$$y(t) = A\cos(\Omega t + \theta). \tag{3}$$

The damping force-velocity relation of an SVD can be expressed as

$$F_{\mathrm{d}} = c \cdot \mathrm{sign}(\dot{y}(t)) \, |\dot{y}(t)|^{\alpha}. \tag{4}$$

Figure 2 shows the variations in the damping force with time under harmonic excitation of different frequencies. The response velocity of the system is small in the low-frequency region. Therefore, the force induced by the SVD is greater than that induced by the linear viscous damper, while it is smaller than that induced by the linear viscous damper in the high-frequency region. The SVD shows the characteristics of large damping in the low-frequency region and those of small damping in the high-frequency region. This feature is also expected in the developed vibration isolation system.

2.2 Dynamic modeling of the QZS-SVD isolator

Figure 3 shows a schematic of the QZS-SVD isolator. The typical three-spring structure comprises two oblique springs, a vertical spring, and a vertical SVD. When the QZS isolator bears an isolated vibration object, the two oblique springs are compressed along the horizontal direction to provide negative stiffness along the vertical direction. Moreover, the vertical spring is compressed to provide bearing capacity and positive stiffness along the vertical direction. The positive and negative stiffnesses are superimposed, affording QZS and static equilibrium.

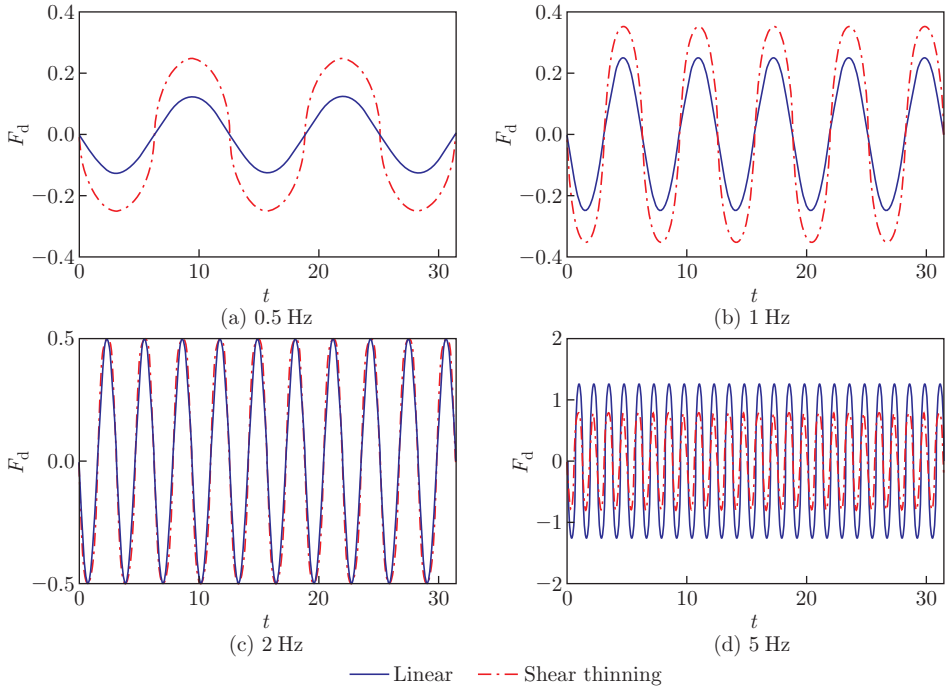

Fig. 2 Variations in the SVD damping force with time under harmonic excitation of different frequencies, where $c = 0.5$, $A = 0.5$, and $\alpha = 0.5$ (color online)

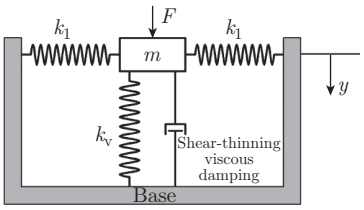

Fig. 3 Schematic of the QZS-SVD isolator

Under an external force F, the isolated object deviates from the equilibrium position and yields a displacement y. The force-displacement relation of the QZS-SVD isolator is expressed as

$$F_{\mathrm{QZS}} = k_{\mathrm{v}} y - 2k_1 y\Big(\frac{L_0}{\sqrt{a^2 + y^2}} - 1\Big), \tag{5}$$

where k_{v} denotes the vertical spring stiffness, k_1 denotes the oblique spring stiffness, L_0 represents the original length of the oblique spring, and a represents the length of the oblique spring when it is compressed along the horizontal direction.

To facilitate the subsequent calculations, Eq. (5) is usually expressed approximately using the following third-order Taylor expansion[12]:

$$F_{\mathrm{QZS}} = \frac{L_0 k_1}{a^3} y^3. \tag{6}$$

Under the action of harmonic excitation $F_{\mathrm{e}} = F\cos(wt)$, the equation of motion can be

expressed as

$$m\ddot{y} + F_{\mathrm{d}} + F_{\mathrm{QZS}} = F\cos(wt). \tag{7}$$

Substituting Eqs. (4) and (6) into Eq. (7), the equation of motion can be expanded as

$$m\ddot{y} + c\mathrm{sign}(\dot{y})\,|\dot{y}|^{\alpha} + \frac{L_0 k_1}{a^3}y^3 = F\cos(wt). \tag{8}$$

Transforming Eq. (8) into a dimensionless form, we achieve

$$\ddot{\overline{y}} + 2\zeta\mathrm{sign}(\dot{\overline{y}})\,\left|\dot{\overline{y}}\right|^{\alpha} + \gamma\overline{y}^3 = \overline{F}\cos(\Omega\tau), \tag{9}$$

where

$$w_0 = \sqrt{\frac{k_{\mathrm{v}}}{m}}, \quad \tau = w_0 t, \quad \zeta = \frac{cw_0}{2k_{\mathrm{v}}}, \quad \Omega = \frac{w}{w_0}, \quad \overline{F} = \frac{F}{k_{\mathrm{v}}L_0},$$
$$\beta = \frac{k_1}{k_{\mathrm{v}}}, \quad \overline{y} = \frac{y}{L_0}, \quad \overline{a} = \frac{a}{L_0}, \quad \gamma = \frac{\beta}{\overline{a}^3}.$$

3 Dynamic analysis

3.1 Amplitude-frequency responses

Equation (9) is a nonlinear ordinary differential equation, in which the stiffness and damping correspond to the third-order nonlinearity and fractional power, respectively. In this study, the HBM is used to approximate the solution to Eq. (9). Let the steady-state periodic response of the system be as follows:

$$\overline{y}(\tau) = A\cos(\Omega\tau + \theta), \tag{10}$$

where A represents the steady-state response amplitude, and θ denotes the response phase.

Substituting Eq. (10) into Eq. (9), we can obtain

$$-\Omega^2 A\cos(\Omega\tau+\theta) - 2\zeta\Omega^{\alpha}A^{\alpha}\mathrm{sign}(\dot{\overline{y}})|\sin(\Omega\tau+\theta)|^{\alpha} + \gamma A^3\cos^3(\Omega\tau+\theta) = \overline{F}\cos(\Omega\tau). \tag{11}$$

Only the influence of the main resonance under harmonic excitation is considered, and the higher-order harmonic term is ignored. The last two terms on the left-hand side of Eq. (11) are subject to Fourier expansion, and the first-order main harmonic term is achieved as

$$\mathrm{sign}(\dot{\overline{y}})|\sin(\Omega\tau+\theta)|^{\alpha} = \frac{2}{\pi}\Big(2 - \Big(2-\frac{\pi}{2}\Big)\alpha\Big)\sin(\Omega\tau+\theta), \tag{12}$$

$$\cos^3(\Omega\tau+\theta) = \frac{1}{4}(3\cos(\Omega\tau+\theta) + \cos 3(\Omega\tau+\theta)). \tag{13}$$

Using Eqs. (12) and (13), the equation of motion can be simplified as

$$\begin{aligned} &-\Omega^2 A\cos(\Omega\tau+\theta) - \Big(\frac{8}{\pi} - \Big(\frac{8}{\pi}-2\Big)\alpha\Big)\zeta\Omega^{\alpha}A^{\alpha}\sin(\Omega\tau+\theta) \\ &+ \frac{3}{4}\gamma A^3\cos(\Omega\tau+\theta) = \overline{F}\cos(\Omega\tau). \end{aligned} \tag{14}$$

Let the coefficients of both $\cos(\Omega\tau+\theta)$ and $\sin(\Omega\tau+\theta)$ be 0. Then, we can obtain

$$\begin{cases} \Big(\frac{3}{4}\gamma A^3 - A\Omega^2\Big)\cos\theta - \Big(\frac{8}{\pi} - \Big(\frac{8}{\pi}-2\Big)\alpha\Big)\zeta\Omega^{\alpha}A^{\alpha}\sin\theta = \overline{F}, \\ -\Big(\frac{8}{\pi} - \Big(\frac{8}{\pi}-2\Big)\alpha\Big)\zeta\Omega^{\alpha}A^{\alpha}\cos\theta - \Big(\frac{3}{4}\gamma A^3 - A\Omega^2\Big)\sin\theta = 0. \end{cases} \tag{15}$$

Eliminating the phase θ in Eq. (15), the amplitude-frequency characteristic equation is obtained as follows:

$$\Big(\frac{3}{4}\gamma A^3 - A\Omega^2\Big)^2 + \Big(\Big(\frac{8}{\pi} - \Big(\frac{8}{\pi}-2\Big)\alpha\Big)\zeta\Omega^{\alpha}A^{\alpha}\Big)^2 = \overline{F}^2. \tag{16}$$

3.2 Numerical analysis

In the previous section, the amplitude-frequency response of the system was obtained using the HBM. This response will also be used to evaluate the vibration isolation performance of the QZS-SVD isolator. It is necessary to verify the correctness of the analytical solution using numerical simulation. The parameters of the QZS-SVD isolator are set as follows: the damping ratio coefficient $\zeta = 0.05$, the damping force index $\alpha = 0.5$, the equivalent stiffness $\gamma = 10$, and the excitation force amplitude $\overline{F} = 0.05$. Moreover, the fourth-order Runge-Kutta method is used to solve the numerical solution to Eq. (9). Figure 4 shows that the analytical solution agrees well with the numerical solution. However, a certain deviation is observed in an ultralow-frequency region.

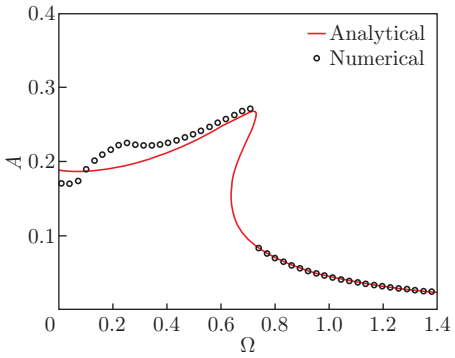

Fig. 4 Comparison between analytical and numerical solutions of the amplitude-frequency response (color online)

The analytical solution obtained using the HBM contains only the first-order harmonic. However, in the ultralow-frequency region, the exact solution of the QZS system may contain complex responses such as superharmonic and subharmonic. To analyze the reason for this error between the analytical and numerical solutions, Fig. 5 shows the simulation results under certain specific frequency ratios ($\Omega = 0.1$, 0.3, 0.5, and 0.7) in the low-frequency range, including the steady-state response and phase diagram. Figures 5(a), 5(c), 5(e), and 5(g) show that when the system is excited using an ultralow frequency, the response is not just a single main harmonic. With the increase in the excitation frequencies, the higher harmonic gradually disappears and exhibits a single harmonic response. Figures 5(b), 5(d), 5(f), and 5(h) show that with the increase in the frequency, the complex shape in the phase diagram gradually changes to an ellipse, and the analytical solution agrees well with the numerical solution. This result explains the deviation between the analytical and numerical solutions in the ultralow-frequency range in Fig. 4.

3.3 Force transmissibility under harmonic excitation

Force transmissibility is generally an important index to evaluate the performance of a vibration isolation system and is used to evaluate the performance of the QZS-VSD isolator under harmonic excitation. The force transmissibility T_{f} is defined as the ratio of the force transmitted to the foundation to the amplitude of the exciting force. The force transmitted to the foundation through the QZS-SVD isolator is

$$F_{\mathrm{t}} = 2\zeta \mathrm{sign}(\dot{\overline{y}})|\dot{\overline{y}}|^{\alpha} + \gamma \overline{y}^{3}. \tag{17}$$

Based on the aforementioned definition, the force transmissibility of the QZS-VSD isolator

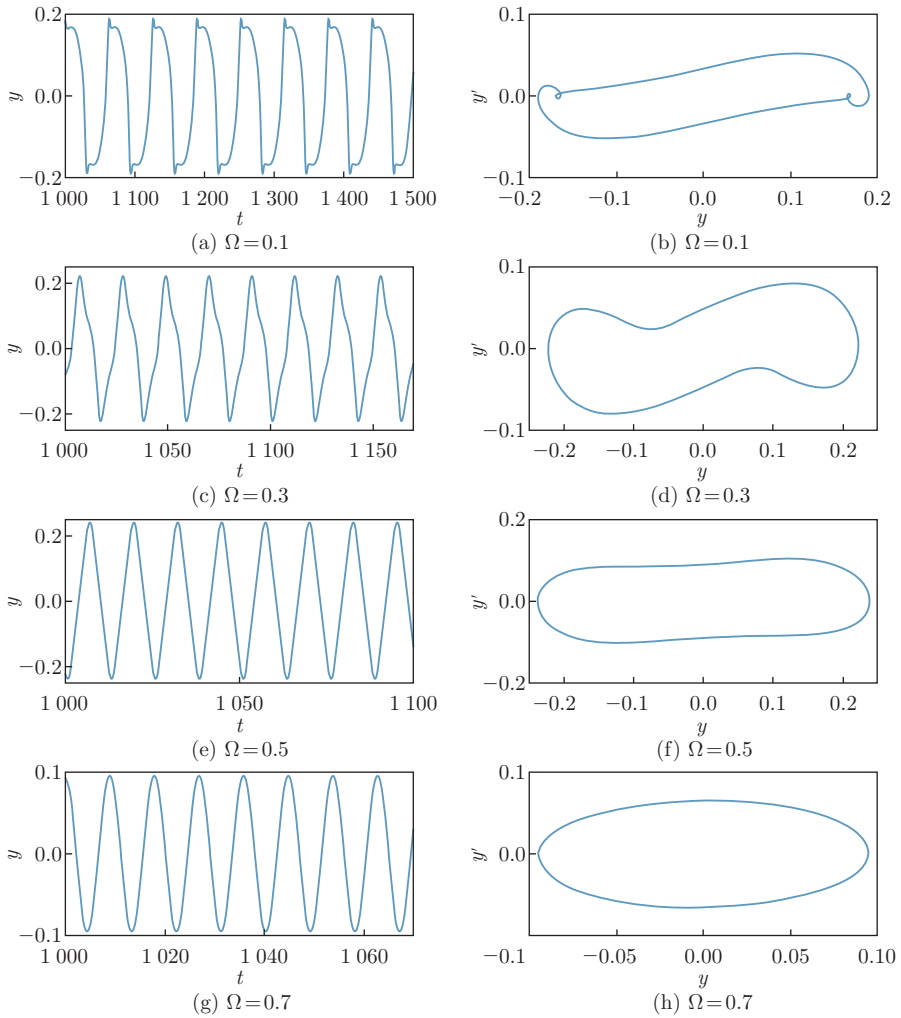

Fig. 5 Time domain diagram and phase trajectories of numerical simulation under different frequencies (color online)

is expressed as[10]

$$T_{\mathrm{f}} = 20\lg\left(\frac{F_{\mathrm{t}}}{F_{\mathrm{e}}}\right) = 20\lg\left(\sqrt{\frac{\left(\left(\frac{8}{\pi}-\left(\frac{8}{\pi}-2\right)\alpha\right)\zeta\Omega^{\alpha}A^{\alpha}\right)^{2}+\left(\frac{3}{4}\gamma A^{3}\right)^{2}}{F_{\mathrm{e}}^{2}}}\right). \tag{18}$$

3.4 Comparison with T-QZS and linear isolators

In this section, the vibration isolation performance of the QZS-SVD isolator is compared with those of T-QZS and linear isolators. In T-QZS isolators, damping is generally considered to be linear, which induces a problem that considering both low-frequency and high-frequency vibration isolations is difficult. Small damping easily causes the amplitude-frequency curve to bend to the right, and then produces a jumping phenomenon, worsening the low-frequency vibration isolation effect. Increasing the damping can improve the low-frequency vibration isolation, but the effect worsens in the middle- and high-frequency regions. Alternatively, the shear-thinning viscous damping varies nonlinearly with the velocity. Figure 6 shows a comparison of the force transmissibility-frequency curves of the three isolators. Under the same

parameters, the QZS-SVD isolator achieves a very low initial isolation frequency, compared with the T-QZS isolator, thus eliminating the resonance peak and jumping phenomenon in the low-frequency range. As the frequency increases, the transmissibility curve of the QZS-SVD isolator in the high-frequency range is below that of the T-QZS isolator, thus showing better vibration isolation performance. At high frequencies, the force transmissibility curves of the two isolators gradually coincide, and the two isolators show good vibration isolation performance, thereby achieving satisfactory results. The QZS-SVD isolator shows excellent vibration isolation performance and can well isolate vibration in the full-frequency range.

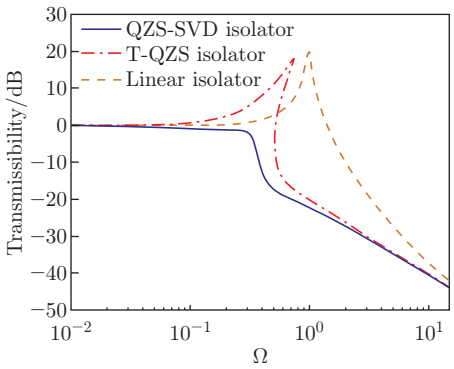

Fig. 6 Comparison of force transmissibility curves of the three vibration isolators, where $\gamma = 10$, $\zeta = 0.05$, $\alpha = 0.5$, and $\overline{F} = 0.02$ (color online)

4 Parameter analysis

The vibration isolation performance of the QZS isolator is affected by the damping ratio coefficient, the stiffness, and the amplitude of excitation force, as well as changes in the variation of the damping force index. This is because the response amplitude determined using Eq. (17) is a function of these parameters. In this section, the effects of the parameters (the damping force index α, the damping ratio coefficient ζ, the excitation force amplitude $\overline{F}$, and the equivalent stiffness γ) on the vibration isolation performance of the QZS-SVD isolator are analyzed.

4.1 Damping force index

Figure 7 shows the force transmissibility curves of the QZS-SVD isolator with different values of the damping force index α. When $\alpha = 1$, the force transmissibility curve represents a T-QZS isolator with linear damping. When $\alpha = 0.8$, compared with the T-QZS isolator, the QZS-SVD isolator mainly suppresses part of the resonance peak, and the improvement in the vibration isolation performance is unnoticeable. With the decrease in the damping force index, the rightward bending phenomenon of the force transmissibility curve weakens in the low-frequency range. When $\alpha = 0.6$, the jumping phenomenon disappears and the resonance peak of the system drops to a very low level. When $\alpha = 0.5$, the resonant peak disappears completely, and the QZS-SVD isolator exhibits a very low initial isolation frequency. When $\alpha = 0.4$, the force transmissibility of the QZS-SVD isolator can be reduced to -20 dB at the frequency ratio of 0.3, isolating more than 90% of the vibration and exhibiting excellent passive vibration isolation performance in the low-frequency region. Generally, when α is small, the vibration isolation performance of the QZS-SVD isolator is enhanced, especially in the low-frequency region. Despite this face, the value of α often depends on the characteristics of the shear-thinning viscous fluid.

4.2 Damping ratio coefficient

Figure 8 shows the force transmissibility curves of the QZS-SVD isolator with different damping ratios. It can be seen that when the damping ratio is small, the curve bending to the right affords a poor low-frequency vibration isolation performance of the system. With the increase in the damping ratio coefficient, the damping force of the SVD increases. The large damping can suppress the formant in the low-frequency region, but increase the force transmissibility in the high-frequency region, consistent with the law of the damping ratio parameter analysis of the T-QZS isolator.

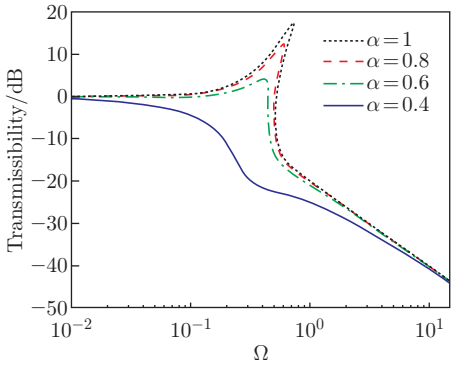

Fig. 7 Force transmissibility curves of the QZS-SVD isolator under different damping force indexes, where $\gamma = 10$, $\zeta = 0.05$, and $\overline{F} = 0.02$ (color online)

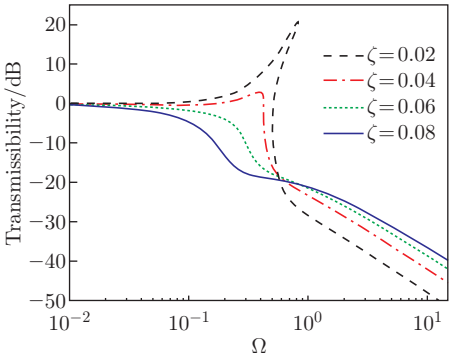

Fig. 8 Force transmissibility curves of the QZS-SVD isolator under different damping ratio coefficients, where $\gamma = 10$, $\alpha = 0.5$, and $\overline{F} = 0.02$ (color online)

Figure 9 shows the amplitude-frequency curves of the QZS-SVD and T-QZS isolators with different damping ratio coefficients. As shown in Fig. 9(a), when $\zeta = 0.01$, the amplitude-frequency curves are considerably bent to the right, and the low-frequency vibration isolation performance is poor. As shown in Fig. 9(b), when $\zeta = 0.03$, the bending degree of the amplitude frequency curve of the T-QZS isolator is weakened, and that of the QZS-SVD isolator improves considerably. Furthermore, the jumping phenomenon is almost completely eliminated. As shown in Fig. 9(c), when $\zeta = 0.05$, the QZS-SVD isolator completely eliminates the formant and shows good low-frequency vibration isolation performance. As shown in Fig. 9(d), when $\zeta = 0.12$, the T-QZS isolator eliminates the jump phenomenon and reduces the initial isolation frequency ratio to about 0.5, while the QZS-SVD isolator shows a better vibration isolation performance in the low-frequency region. However, the high-frequency vibration isolation performance of the two types of vibration isolators deteriorates because of an increase in the damping ratio. In Fig. 10, the force transmissivity curves of the two isolators are compared. The value of the critical damping ratio ζ at the time of the elimination of the jump phenomenon is considered. The QZS-SVD isolator not only shows slightly better vibration isolation performance than the T-QZS isolator in the low-frequency region, but also shows better performance in the middle- and high-frequency regions, where the force transmissivity of the QZS-SVD isolator can be lower than that of the T-QZS isolator by 10 dB or more. In the QZS-SVD isolator, an appropriate value of the damping ratio can be selected to simultaneously obtain good isolation performance in low- and high-frequency regions.

4.3 Excitation amplitude

Figure 11 shows the force transmissibility curve of the QZS-VSD isolator under different excitation amplitudes. With the increase in the excitation amplitude, the resonance peak and initial vibration isolation frequency increase gradually, deteriorating the low-frequency isolation

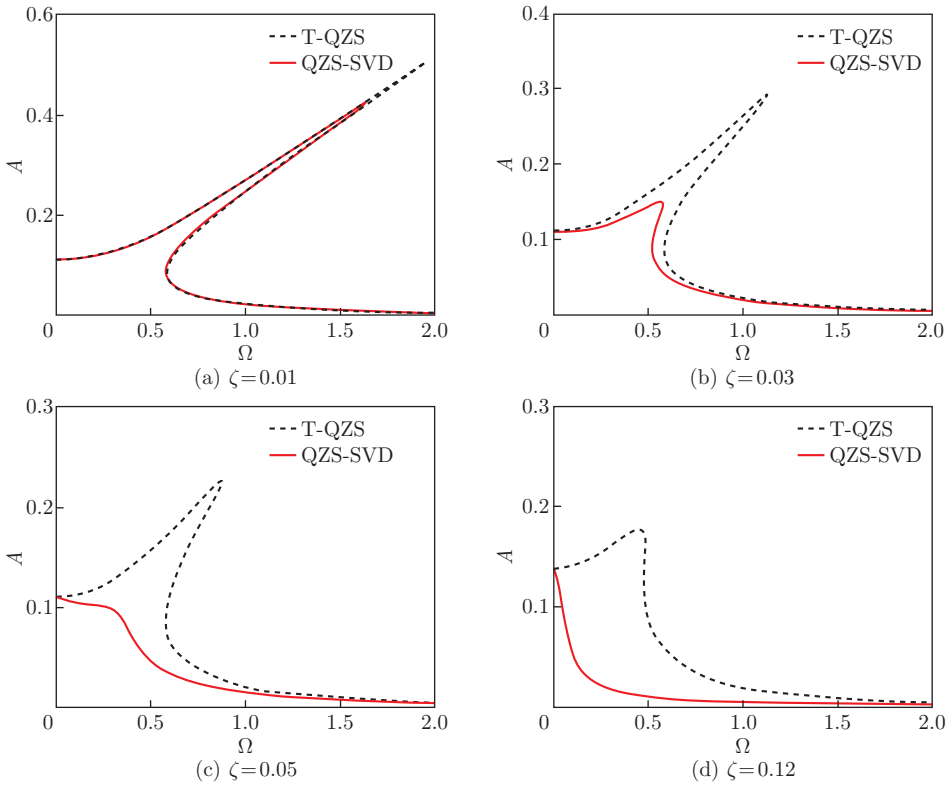

Fig. 9 Amplitude-frequency curves of the QZS-SVD and T-QZS isolators with different damping ratio coefficients, where $\gamma = 10$, $\alpha = 0.5$, and $\overline{F} = 0.02$ (color online)

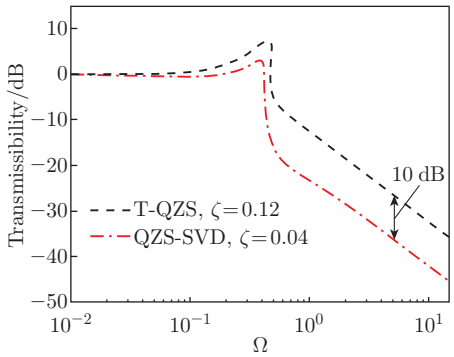

Fig. 10 Force transmissibility curves under different critical damping ratios, where $\gamma = 10$, $\alpha = 0.5$, and $\overline{F} = 0.02$ (color online)

performance. However, the high-frequency is not affected, similar to the variation law of linear damping QZS. When the peak frequency Ω_{d} of the QZS isolator is not greater than the resonant frequency of the corresponding linear system ($\Omega = 1$), the performance of the QZS isolator is better than that of the linear system. When $\Omega_{\mathrm{d}} = 1$, the excitation force amplitude is called the critical excitation force amplitude F_{cr}. When $\overline{F} < F_{\mathrm{cr}}$, the vibration isolation performance of the QZS system is better than that of the linear system.

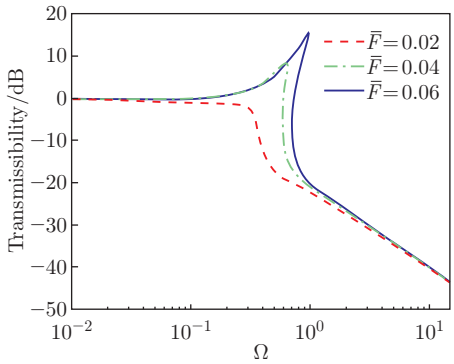

Fig. 11 Force transmissibility curves of the QZS-VSD isolator under different excitation amplitudes, where $\gamma = 10$, $\alpha = 0.5$, and $\zeta = 0.05$ (color online)

Figure 12 shows a comparison between the QZS-SVD and T-QZS isolators under different excitation amplitudes. As shown in Fig. 12(a), when $\overline{F} = 0.02$, the amplitudes of both isolators are smaller than the critical excitation force amplitude, and the performance of the QZS-SVD isolator is considerably better than that of the T-QZS isolator. With the increase in the excitation amplitude, as shown in Fig. 12(b) when $\overline{F} = 0.036$, the T-QZS isolator reaches the critical excitation amplitude, and the vibration isolation performance is poor compared with

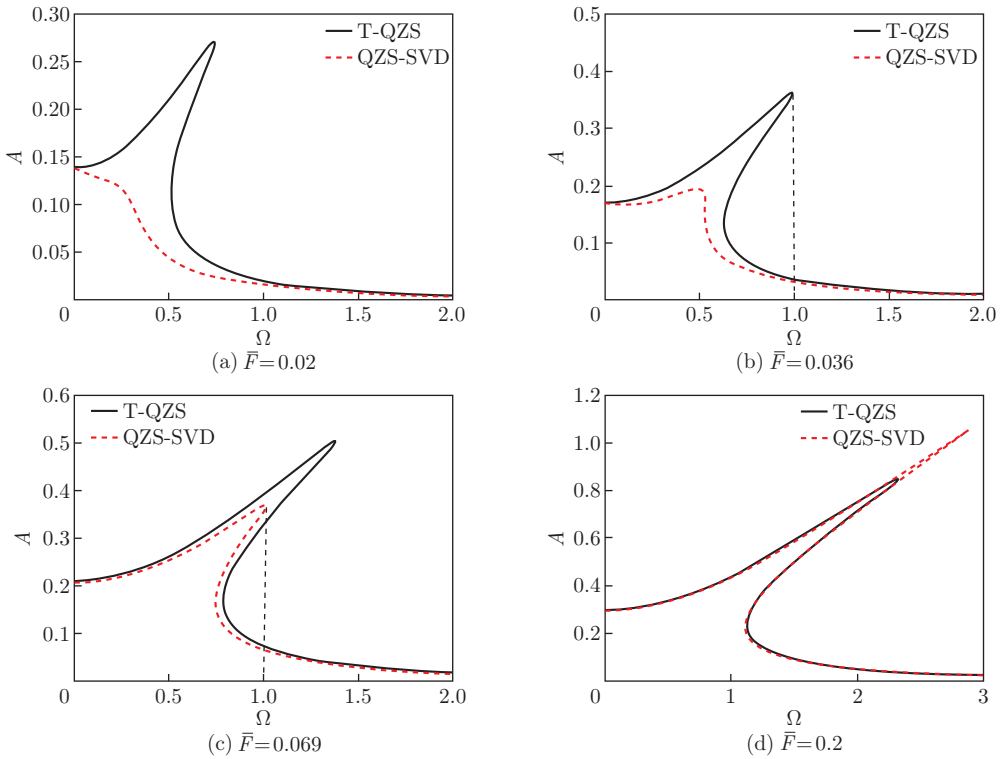

Fig. 12 Comparison between the QZS-SVD and T-QZS isolators under different excitation amplitudes, where $\gamma = 10$, $\alpha = 0.5$, and $\zeta = 0.05$ (color online)

the corresponding linear system. This also reflects the problem that the vibration isolation performance of the QZS isolator deteriorates in the case of large excitation. In the QZS-SVD isolator, the right bending and peak value in the amplitude-frequency curve can be better controlled. As shown in Fig. 12(c), when $\overline{F} = 0.069$, the QZS-SVD isolator reaches the critical excitation amplitude, and the vibration isolation performance of the QZS-SVD isolator starts to deteriorate compared with the linear systems. In Fig. 12(d), when $\overline{F} = 0.2$, the right bending of the amplitude-frequency curve of the SVD is substantial and exceeds the bending degree of the linear damping QZS isolator. The excessive excitation amplitude is assumed to promote the enhancement of the damping shear-thinning effect. However, the vibration isolation performance of the QZS system is far inferior to that of the linear vibration isolator in this interval, and hence it is not discussed. Compared with the T-QZS isolator, the critical excitation amplitude of the QZS-SVD isolator increases by 92%, which (to some extent) solves the problem of the deterioration of the vibration isolation performance caused by the hardening stiffness characteristics of the T-QZS isolator when the amplitude is very large.

4.4 Equivalent stiffness

Generally, with the decrease in the equivalent stiffness, the bending degree of the force transmissibility curve decreases, while the resonance peak value and initial isolation frequency gradually decrease, increasing the effective isolation frequency domain and improving the isolation performance of the system. Figure 13 shows the force transmissivity curves of the QZS-SVD and T-QZS isolators with different values of the equivalent stiffness when $\alpha = 0.5$. Both isolators follow the aforementioned laws. When $\gamma = 20$, the force transmissivity curve of the T-QZS vibration isolator bends considerably to the right, the initial vibration isolation frequency ratio reaches 0.88, and the low-frequency vibration isolation performance is poor. However, no right bending and resonance peak are observed in the case of the QZS-SVD isolator. Further, the force transmissibility of the vibration isolation can be reduced rapidly when the frequency ratio is 0.4. When $\gamma = 10$, the bending degree of the T-QZS curve decreases, the initial isolation frequency ratio decreases to about 0.74, and the curve of the QZS-SVD isolator shifts to the left by less than 0.1. When $\gamma = 1$, the initial isolation frequency ratio of the T-QZS isolator reduces to about 0.4, while that of the QZS-SVD isolator reduces to about 0.2 and can rapidly attenuate. Thus, when γ is large, the QZS-SVD isolator shows better vibration isolation performance than the T-QZS isolator. A small γ implies that the QZS curve of the QZS isolators is smoother at the static equilibrium position and shows a wider effective QZS range compared with a large γ. Scholars have conducted considerable research to obtain QZS isolators with a wide QZS range. However, the structure of these isolators is usually more complex than those of the T-QZS isolators[28–29]. The SVD can significantly improve the vibration isolation performance of the QZS vibration isolators using a simple structure and a large equivalent stiffness.

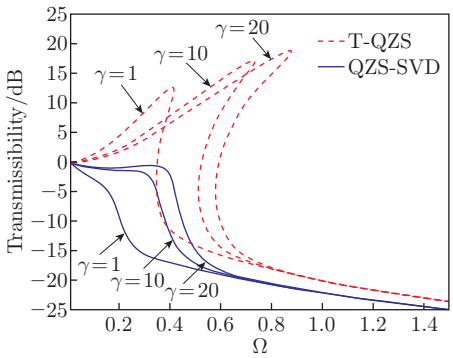

Fig. 13 Force transmissivity curves of the QZS-SVD and T-QZS isolators under different equivalent stiffnesses, where $\zeta = 0.05$, $\alpha = 0.5$, and $\overline{F} = 0.02$ (color online)

5 Conclusions

In this study, a QZS vibration isolator with a SVD is studied. The mathematical model for the QZS-SVD isolator is established, which is a dynamic system with nonlinear stiffness and damping. The HBM is employed to obtain the amplitude-frequency characteristics of the QZS-SVD isolator, and the correctness of the analytical solution is verified using numerical simulation. The force transmissibility is used to evaluate the vibration isolation performance of the system, which is compared with those of the T-QZS and linear stiffness systems. Finally, the effects of the damping force index, the damping ratio, the excitation amplitude, and the nonlinear stiffness on the vibration isolation performance of the system are discussed. The following conclusions can be drawn.

(i) Under harmonic excitation, the SVD shows large damping in the low-frequency region and small damping in the high-frequency region. Compared with the T-QZS vibration isolator, the QZS-SVD vibration isolator shows the lower initial vibration isolation frequency and resonance peak, exhibiting excellent ultralow-frequency vibration isolation performance. Ideally, it can completely eliminate the jump phenomenon or even the resonance peak.

(ii) In the QZS-SVD isolator, an appropriate value of the damping ratio can be selected to obtain enhanced vibration isolation performance in the low-frequency region as well as medium- to high-frequency regions. At medium and high frequencies, the force transmissibility of the QZS-SVD isolator is more than 10 dB lower than that of the T-QZS isolator.

(iii) The QZS-SVD isolator shows a larger critical excitation amplitude than the T-QZS isolator, thus improving the problem of the deterioration of the vibration isolation performance owing to the hardening stiffness characteristics of the T-QZS isolator when the amplitude is very large.

References

[1] IBRAHIM, R. A. Recent advances in nonlinear passive vibration isolators. *Journal of Sound and Vibration*, **314**(3-5), 371–452 (2008)

[2] LIU, J., CHEN, T., ZHANG, Y., WEN, G., QING, Q., WANG, H., SEDAGHATI, R., and XIE, Y. M. On sound insulation of pyramidal lattice sandwich structure. *Composite Structures*, **208**, 385–394 (2019)

[3] ZHANG, S. J., TO, S., ZHANG, G. Q., and ZHU, Z. W. A review of machine-tool vibration and its influence upon surface generation in ultra-precision machining. *International Journal of Machine Tools & Manufacture*, **91**, 34–42 (2015)

[4] LI, L., TAN, L., KONG, L., WANG, D., and YANG, H. The influence of flywheel micro vibration on space camera and vibration suppression. *Mechanical Systems and Signal Processing*, **100**, 360–370 (2018)

[5] ZHOU, J., WANG, K., XU, D., OUYANG, H., and FU, Y. Vibration isolation in neonatal transport by using a quasi-zero-stiffness isolator. *Journal of Vibration and Control*, **24**(15), 3278–3291 (2018)

[6] RIVIN, E. Passive vibration isolation. *Applied Mechanics Reviews*, **57**(6), B31–B32 (2004)

[7] ALABUZHEV, P. M. and RIVIN, E. I. *Vibration Protecting and Measuring Systems with Quasi-Zero Stiffness*, Hemisphere Publishing, New York, 21–90 (1989)

[8] CARRELLA, A., BRENNAN, M. J., and WATERS, T. P. Static analysis of a passive vibration isolator with quasi-zero-stiffness characteristic. *Journal of Sound and Vibration*, **301**(3-5), 678–689 (2007)

[9] CARRELLA, A., BRENNAN, M. J., KOVACIC, I., and WATERS, T. P. On the force transmissibility of a vibration isolator with quasi-zero-stiffness. *Journal of Sound and Vibration*, **322**(4-5), 707–717 (2009)

[10] KOVACIC, I., BRENNAN, M. J., and WATERS, T. P. A study of a nonlinear vibration isolator with a quasi-zero stiffness characteristic. *Journal of Sound and Vibration*, **315**(3), 700–711 (2008)

[11] KOVACIC, I., BRENNAN, M. J., and LINETON, B. Effect of a static force on the dynamic behaviour of a harmonically excited quasi-zero stiffness system. *Journal of Sound and Vibration*, **325**(4-5), 870–883 (2009)

[12] XU, D., ZHANG, Y., ZHOU, J., and LOU, J. On the analytical and experimental assessment of the performance of a quasi-zero-stiffness isolator. *Journal of Vibration and Control*, **20**(15), 2314–2325 (2014)

[13] LAN, C. C., YANG, S. A., and WU, Y. S. Design and experiment of a compact quasi-zero-stiffness isolator capable of a wide range of loads. *Journal of Sound and Vibration*, **333**(20), 4843–4858 (2014)

[14] LIU, X., HUANG, X., and HUA, H. On the characteristics of a quasi-zero stiffness isolator using Euler buckled beam as negative stiffness corrector. *Journal of Sound and Vibration*, **332**(14), 3359–3376 (2013)

[15] NIU, F., MENG, L., WU, W., SUN, J., ZHANG, W., MENG, G., and RAO, Z. Design and analysis of a quasi-zero stiffness isolator using a slotted conical disk spring as negative stiffness structure. *Journal of Vibroengineering*, **16**(4), 1769–1785 (2014)

[16] ZHOU, J., WANG, X., XU, D., and BISHOP, S. Nonlinear dynamic characteristics of a quasi-zero stiffness vibration isolator with cam-roller-spring mechanisms. *Journal of Sound and Vibration*, **346**, 53–69 (2015)

[17] ZHOU, J., XIAO, Q., XU, D., OUYANG, H., and LI, Y. A novel quasi-zero-stiffness strut and its applications in six-degree-of-freedom vibration isolation platform. *Journal of Sound and Vibration*, **394**, 59–74 (2017)

[18] ZHOU, J., XU, D., and BISHOP, S. A torsion quasi-zero stiffness vibration isolator. *Journal of Sound and Vibration*, **338**, 121–133 (2015)

[19] ZENG, R., WEN, G., ZHOU, J., and ZHAO, G. Limb-inspired bionic quasi-zero stiffness vibration isolator. *Acta Mechanica Sinica*, **37**(7), 1155–1170 (2021)

[20] ROBERTSON, W. S., KIDNER, M. R. F., CAZZOLATO, B. S., and ZANDER, A. C. Theoretical design parameters for a quasi-zero stiffness magnetic spring for vibration isolation. *Journal of Sound and Vibration*, **326**(1-2), 88–103 (2009)

[21] WU, W., CHEN, X., and SHAN, Y. Analysis and experiment of a vibration isolator using a novel magnetic spring with negative stiffness. *Journal of Sound and Vibration*, **333**(13), 2958–2970 (2014)

[22] XU, D., YU, Q., ZHOU, J., and BISHOP, S. R. Theoretical and experimental analyses of a nonlinear magnetic vibration isolator with quasi-zero-stiffness characteristic. *Journal of Sound and Vibration*, **332**(14), 3377–3389 (2013)

[23] JIANG, Y., SONG, C., DING, C., and XU, B. Design of magnetic-air hybrid quasi-zero stiffness vibration isolation system. *Journal of Sound and Vibration*, **477**, 1–15 (2020)

[24] LIU, C. and YU, K. A high-static-low-dynamic-stiffness vibration isolator with the auxiliary system. *Nonlinear Dynamics*, **94**(3), 1549–1567 (2018)

[25] FENG, X., JING, X., XU, Z., and GUO, Y. Bio-inspired anti-vibration with nonlinear inertia coupling. *Mechanical Systems and Signal Processing*, **124**, 562–595 (2019)

[26] YANG, J., JIANG, J. Z., and NEILD, S. A . Dynamic analysis and performance evaluation of nonlinear inerter-based vibration isolators. *Nonlinear Dynamics*, **99**(3), 1823–1839 (2020)

[27] LU, Z., YANG, T., BRENNAN, M. J., LIU, Z., and CHEN, L. Q. Experimental investigation of a two-stage nonlinear vibration isolation system with high-static-low-dynamic stiffness. *Journal of Applied Mechanics*, **84**(2), 021001 (2017)

[28] WANG, X., ZHOU, J., XU, D., OUYANG, H., and DUAN, Y. Force transmissibility of a two-stage vibration isolation system with quasi-zero stiffness. *Nonlinear Dynamics*, **87**(1), 633–646 (2017)

[29] ZHAO, F., JI, J. C., YE, K., and LUO, Q. Increase of quasi-zero stiffness region using two pairs of oblique springs. *Mechanical Systems and Signal Processing*, **144**, 106975 (2020)

[30] WANG, K., ZHOU, J., CHANG, Y., OUYANG, H., XU, D., and YANG, Y. A nonlinear ultra-low-frequency vibration isolator with dual quasi-zero-stiffness mechanism. *Nonlinear Dynamics*, **101**(2), 755–773 (2020)

[31] DENG, T., WEN, G., DING, H., LU, Z. Q., and CHEN, L. Q. A bio-inspired isolator based on characteristics of quasi-zero stiffness and bird multi-layer neck. *Mechanical Systems and Signal Processing*, **145**, 106967 (2020)

[32] KIM, J., JEON, Y., UM, S., PARK, U., KIM, K. S., and KIM, S. A novel passive quasi-zero stiffness isolator for ultra-precision measurement systems. *International Journal of Precision Engineering and Manufacturing*, **20**(9), 1573–1580 (2019)

[33] WANG, Q., ZHOU, J., XU, D., and OUYANG, H. Design and experimental investigation of ultra-low frequency vibration isolation during neonatal transport. *Mechanical Systems and Signal Processing*, **139**, 106633 (2020)

[34] DING, H., JI, J., and CHEN, L. Q. Nonlinear vibration isolation for fluid-conveying pipes using quasi-zero stiffness characteristics. *Mechanical Systems and Signal Processing*, **121**, 675–688 (2019)

[35] LANG, Z. Q., JING, X. J., BILLINGS, S. A., TOMLINSON, G. R., and PENG, Z. K. Theoretical study of the effects of nonlinear viscous damping on vibration isolation of sdof systems. *Journal of Sound and Vibration*, **323**(1-2), 352–365 (2009)

[36] LV, Q. and YAO, Z. Analysis of the effects of nonlinear viscous damping on vibration isolator. *Nonlinear Dynamics*, **79**(4), 2325–2332 (2015)

[37] MOFIDIAN, S. M. M. and BARDAWEEL, H. Displacement transmissibility evaluation of vibration isolation system employing nonlinear-damping and nonlinear-stiffness elements. *Journal of Vibration and Control*, **24**(18), 4247–4259 (2018)

[38] LIU, C., TANG, J., YU, K., LIAO, B., HU, R., and ZANG, X. On the characteristics of a quasi-zero-stiffness vibration isolator with viscoelastic damper. *Applied Mathematical Modelling*, **88**, 367–381 (2020)

[39] ZHANG, Z., NIU, M., YUAN, K., and ZHANG, Y. Research on linear/nonlinear viscous damping and hysteretic damping in nonlinear vibration isolation systems. *Applied Mathematics and Mechanics* (*English Edition*), **41**(7), 983–998 (2020) https://doi.org/10.1007/s10483-020-2630-6

[40] DHOLE, S. D., CHHABRA, R. P., and ESWARAN, V. Flow of power-law fluids past a sphere at intermediate Reynolds numbers. *Industrial & Engineering Chemistry Research*, **45**(13), 4773–4781 (2006)

[41] IYER, S. S., VEDAD-GHAVAMI, R., LEE, H., LIGER, M., KAVEHPOUR, H. P., and CANDLER, R. N. Nonlinear damping for vibration isolation of microsystems using shear thickening fluid. *Applied Physics Letters*, **102**(25), 251902 (2013)